

Nickel–Carbon Bond Oxygenation with Green Oxidants via High-Valent Nickel Species

Chi-Herng Hu, Seoung-Tae Kim, Mu-Hyun Baik,* and Liviu M. Mirica*



Cite This: *J. Am. Chem. Soc.* 2023, 145, 11161–11172



Read Online

ACCESS |



Metrics & More

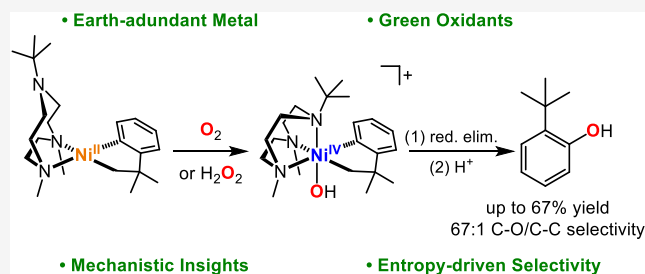


Article Recommendations



Supporting Information

ABSTRACT: Described herein is the synthesis of the Ni^{II} complex (tBuMe₂tacn)Ni^{II}(cycloneophyl) (tBuMe₂tacn = 1-tert-butyl-4,7-dimethyl-1,4,7-triazacyclononane, cycloneophyl = –CH₂CMe₂-o-C₆H₄–) and its reactivity with dioxygen and peroxides. The new tBuMe₂tacn ligand is designed to enhance the oxidatively induced bond-forming reactivity of high-valent Ni intermediates. Tunable chemoselectivity for Csp²–O vs Csp²–Csp³ bond formation was achieved by selecting the appropriate solvent and reaction conditions. Importantly, the use of cumene hydroperoxide and *meta*-chloroperbenzoic acid suggests a heterolytic O–O bond cleavage upon reaction with (tBuMe₂tacn)Ni^{II}(cycloneophyl). Mechanistic studies using isotopically labeled H₂O₂ support the generation of a high-valent Ni-oxygen species via an inner-sphere mechanism and subsequent reductive elimination to form the Csp²–O bond. Kinetic studies of the exceptionally fast Csp²–O bond-forming reaction reveal a first-order dependence on both (tBuMe₂tacn)Ni^{II}(cycloneophyl) and H₂O₂, and thus an overall second-order reaction. Eyring analysis further suggests that the oxidation of the Ni^{II} complex by H₂O₂ is the rate-determining step, which can be modulated by the presence of coordinating solvents. Moreover, computational studies fully support the conclusions drawn from experimental results. Overall, this study reveals for the first time the ability to control the oxidatively induced C–C vs C–O bond formation reactions at a Ni center. Importantly, the described system merges the known organometallic reactivity of Ni with the biomimetic oxidative transformations resembling oxygenases and peroxidases, and involving high-valent metal-oxygen intermediates, which is a novel approach that should lead to unprecedented oxidative catalytic transformations.



INTRODUCTION

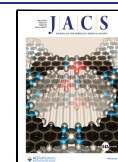
The formation of carbon–oxygen bonds is an important chemical transformation because of the prevalence of hydroxyl and ether functionalities in natural products¹ and polymer precursors.^{2,3} In pursuit of greener chemistry, transition-metal-catalyzed hydroxylation and alkoxylation reactions have emerged as an alternative to traditional stoichiometric synthesis.⁴ In this context, palladium-catalyzed ligand-directed C–H oxygenation has attracted high scientific interest for decades, owing to the ability of Pd to activate strong C–H bonds with predictable site selectivity.⁵ Moreover, the use of dioxygen or hydrogen peroxide as oxidants in C–H hydroxylation reactions has recently been demonstrated in Pd-catalyzed late-stage functionalization,^{6,7} showing the viability of sustainable transformations in building molecular complexity.

On the contrary, the application of nickel, the earth-abundant congener of palladium, as a catalyst in the field of C–H oxygenation has been limited, likely due to challenges in nickel-assisted C–H activation and inherently unstable high-valent nickel species.^{8–10} Nevertheless, numerous efforts have been dedicated to the study of high-valent Ni centers, which are generated chemically,^{11–20} photochemically,^{20,21} or electrochemically,²² to promote C–heteroatom bond formation

reactions.²³ A seminal work by Sanford and Camasso in 2015 showed the capability of multidentate ligands to allow the isolation of well-defined organometallic Ni^{IV} complexes.¹⁶ These isolated Ni^{IV} complexes exhibit uncommon Csp³–X bond-forming reactivity (X = O, S, N) in the presence of exogenous nucleophiles, suggesting a great potential for Ni^{II/IV} catalysis. Multidentate ligands such as 1,4,7-trimethyl-1,4,7-triazacyclononane (Me₃tacn) and pyridinophane (R^N4) ligands have been employed by our group to stabilize high-valent Ni and Pd complexes, with an emphasis on their aerobic reactivity.^{13,14,24–26} Specifically, we observed the rapid oxidation of the LNi^{II}(cycloneophyl) complexes (L = Me₃tacn or R^N4; cycloneophyl = –CH₂CMe₂-o-C₆H₄–) upon exposure to O₂ or H₂O₂, and formation of the corresponding high-valent species (Figure 1). However, the yields of C–C or C–O coupled products resulting from subsequent reductive

Received: January 27, 2023

Published: May 15, 2023



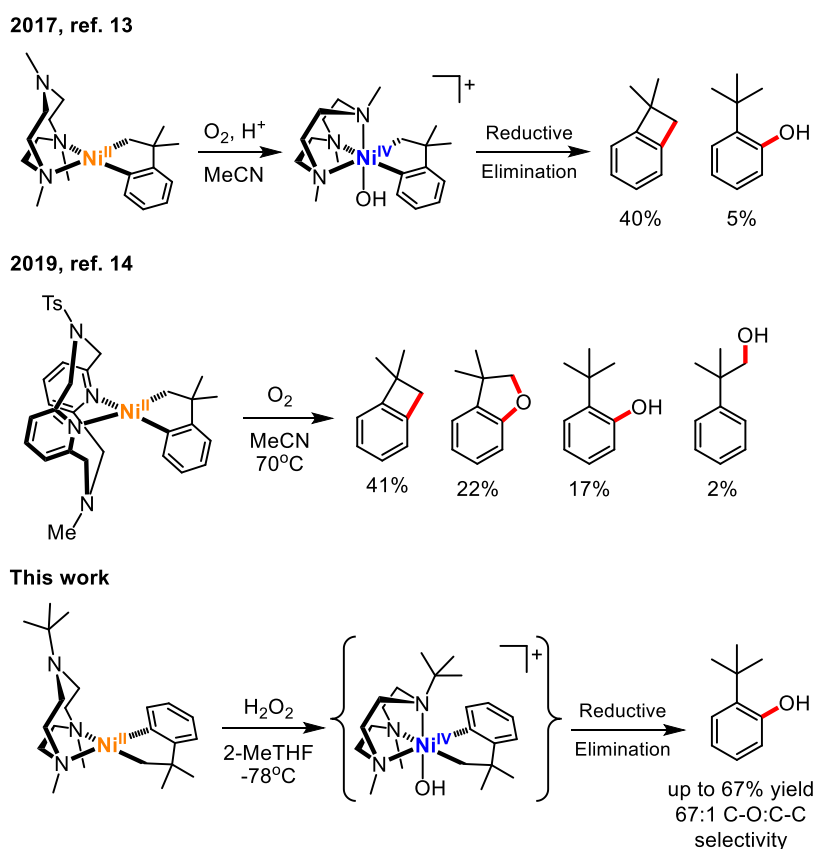


Figure 1. Oxidative C–O bond formation on organometallic nickel complexes induced by molecular oxygen or hydrogen peroxide.

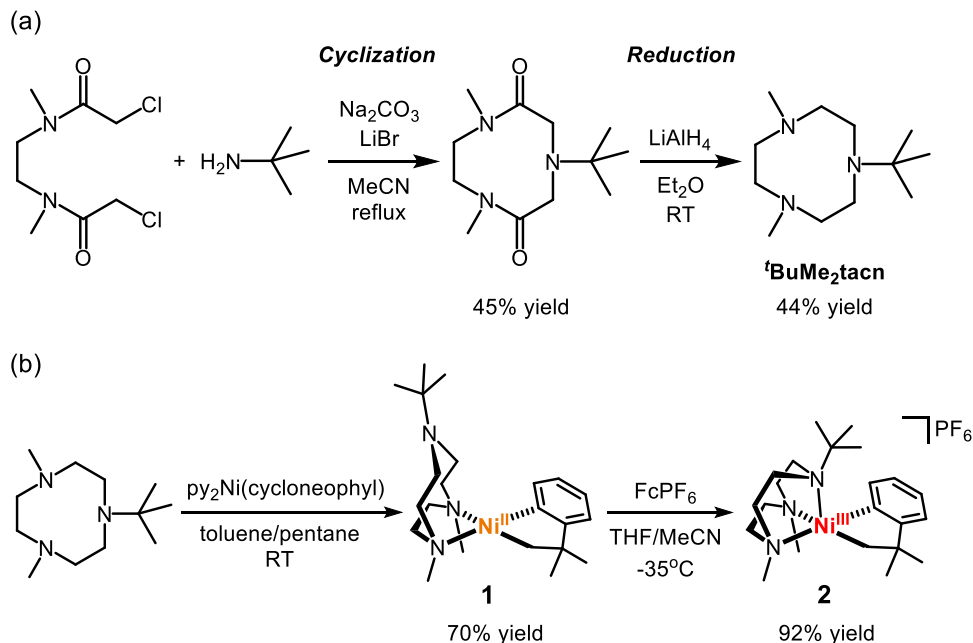


Figure 2. Synthesis of (a) the new ligand ^tBuMe₂tacn and (b) complexes **1** and **2**.

elimination were low and marred by poor chemoselectivity, likely due to an appreciable stabilization of the high-valent Ni species by the strong binding of the axial amine donors to the Ni center. Therefore, we hypothesized that the use of an asymmetric tacn-derived ligand bearing one bulky *tert*-butyl N-substituent could facilitate the reductive elimination from the Ni^{IV} intermediate due to the weaker axial Ni–N_{axial} interaction.

Herein, we report the development of the new 1-*tert*-butyl-4,7-dimethyl-1,4,7-triazacyclononane (^tBuMe₂tacn) ligand and the reactivity of the corresponding Ni complexes. By weakening the interaction of the Ni center with one of the amine donors on the ligand via installing a bulky *tert*-butyl substituent, we were able to accomplish selective, oxidatively induced Csp²–O bond formation in good yields using green

oxidants such as O_2 and H_2O_2 . Moreover, detailed mechanistic studies were conducted to probe the intermediacy of Ni^{IV} intermediates and their reactivity. Kinetic studies reveal a rate-determining oxidation of the Ni^{III} complex by H_2O_2 , while the choice of solvent also plays an important role. Finally, density functional theory (DFT) calculations were employed to provide insights into the molecular structure of transition states and the source of the observed C–O vs C–C chemoselectivity.

RESULTS AND DISCUSSION

Synthesis and Characterization of tBuMe_2tacn and $({}^tBuMe_2tacn)Ni(cycloneophyl)$ Complexes. 1,4,7-Triaza-cyclononane (*tacn*) derivatives are nine-membered macrocycles that have been frequently employed as supporting ligands in transition-metal-catalyzed reactions.^{27,28} In 2017, our group showed that Me_3tacn serves as an excellent ancillary ligand to accommodate organometallic nickel complexes in the Ni^{II} , Ni^{III} , and Ni^{IV} oxidation states.¹³ Nevertheless, the corresponding high-valent Ni complexes exhibit limited bond-forming reactivity. Previous reports have shown that bulky substituents on the axial amine arms are beneficial for reductive elimination at high-valent metal centers.^{14,26,29} As a result, we have developed the asymmetric ligand 1-*tert*-butyl-4,7-dimethyl-1,4,7-triazacyclononane (tBuMe_2tacn) with an anticipation that the amine arm bearing the bulky *tert*-butyl group could destabilize the high-valent Ni intermediates by distorting the coordination geometry and promote the formation of more reactive five-coordinate species.

The tBuMe_2tacn ligand was prepared via a modified crab-like route starting from bischloroacetamide and *tert*-butyl amine (Figure 2a).^{30,31} The cyclized diamide was then reduced by $LiAlH_4$, and final purification of the ligand via vacuum distillation afforded tBuMe_2tacn as a colorless liquid in 20% overall yield. Surprisingly, the tBuMe_2tacn ligand has never been synthesized to date, likely due to the unfavorable cyclization of dimethyl-substituted bischloroacetamide with primary amines.³¹

The complex $({}^tBuMe_2tacn)Ni^{III}(cycloneophyl)$ (**1**) was prepared using a modified literature procedure and obtained as a yellow crystalline solid in 70% yield (Figure 2b).³² The solid-state structure of **1** displays a square planar geometry around the Ni center that resembles $(Me_3tacn)Ni^{III}(cycloneophyl)$ (Figure 3a).¹³ The tBuMe_2tacn ligand coordinates in a κ^2 binding mode, where the amine arm bearing the *tert*-butyl group points away from the Ni center. NMR analysis of **1** suggests an asymmetric and locked-into-place *tacn* backbone structure in solution, as the three ethylene bridges exhibit distinct and well-defined resonance peaks in addition to the two chemically inequivalent N-Me groups. This contrasts with $(Me_3tacn)Ni^{III}(cycloneophyl)$, for which the ethylene peaks are broad, and only one singlet peak was observed for all three N-Me groups, due to their fluxionality on the NMR time scale even at low temperatures.

The cyclic voltammogram (CV) of **1** exhibits two irreversible oxidative waves at -0.383 and 0.153 V vs $Fc^{0/+}$, as well as an irreversible reductive wave at -1.051 V vs $Fc^{0/+}$ (Figure 4a). Based on our previous detailed studies focusing on the redox properties of related Ni and Pd complexes supported by flexible multidentate ligands,^{13,14,24–26,29,33–35} we tentatively assign these features to the oxidation of **1** to $[({}^tBuMe_2tacn)Ni^{III}(cycloneophyl)]^+$, the oxidation of $[(\kappa^3-{}^tBuMe_2tacn)Ni^{III}(cycloneophyl)]^+$ to $[(\kappa^3-{}^tBuMe_2tacn)Ni^{IV}(cycloneophyl)]^{2+}$ —in which the tBuMe_2tacn ligand adopts a κ^3 binding mode, and the reduction of $[(\kappa^3-{}^tBuMe_2tacn)Ni^{III}(cycloneophyl)]^+$ to **1**. The large separation between the $Ni^{II/III}$ redox potentials is attributed to intramolecular structural changes involving the coordination of the bulky *tert*-butyl amine to the Ni center. The small anodic feature at -0.95 V vs $Fc^{0/+}$ likely corresponds to the oxidation of a trace amount of the $[(\kappa^3-{}^tBuMe_2tacn)Ni^{III}(cycloneophyl)]^+$ conformation of **1** being present in solution. Moreover, when the scan rate was increased 10-fold, from 0.1 to 1 V s^{-1} , the oxidative peak potential of **1** at -0.383 V shifts by 72 mV and

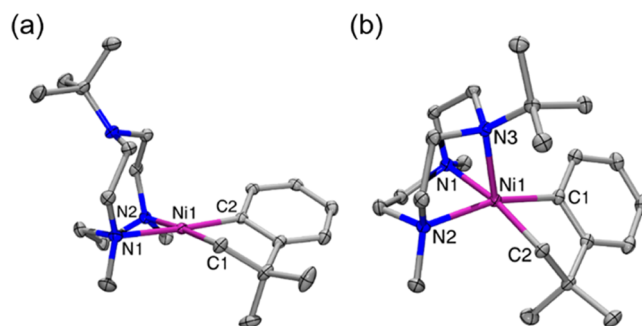


Figure 3. ORTEP representation (50% probability thermal ellipsoids) of (a) complex **1** and (b) complex **2**. The counterions are omitted for simplicity. Selected bond lengths (Å) and angles ($^\circ$): **1**, Ni1–C1 1.937(1), Ni1–C2 1.903(1), Ni1–N1 2.068(1), Ni1–N2 2.048(1), C1–Ni1–N2 175.32(4), C2–Ni1–N1 174.65(4); **2**, Ni1–C1 1.968(1), Ni1–C2 1.972(1), Ni1–N1 2.0829(8), Ni1–N2 2.1099(8), Ni1–N3 2.1977(9), C1–Ni1–N2 164.05(4), C2–Ni1–N1 166.78(4).

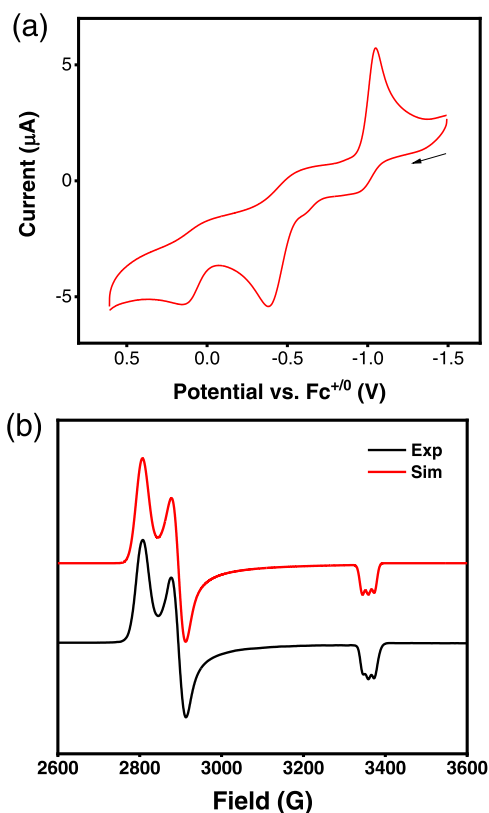


Figure 4. (a) CV of **1** in 0.1 M $nBu_4NPF_6/MeCN$ (scan rate = 100 mV s^{-1}) and (b) experimental and simulated EPR spectra of a frozen 1:3 MeCN/PrCN solution of **2** at 77 K using the following parameters: $g_x = 2.398$, $g_y = 2.324$, $g_z = 2.003$ (A_z (N) = 15.0 G).

the reduction of $[(\kappa^3-{}^tBuMe_2tacn)Ni^{III}(cycloneophyl)]^+$ to **1**. The large separation between the $Ni^{II/III}$ redox potentials is attributed to intramolecular structural changes involving the coordination of the bulky *tert*-butyl amine to the Ni center. The small anodic feature at -0.95 V vs $Fc^{0/+}$ likely corresponds to the oxidation of a trace amount of the $[(\kappa^3-{}^tBuMe_2tacn)Ni^{III}(cycloneophyl)]^+$ conformation of **1** being present in solution. Moreover, when the scan rate was increased 10-fold, from 0.1 to 1 V s^{-1} , the oxidative peak potential of **1** at -0.383 V shifts by 72 mV and

the reductive peak potential of $[(^t\text{BuMe}_2\text{tacn})\text{-Ni}^{\text{III}}(\text{cycloneophyl})]^+$ at -1.051 V shifts by 35 mV, which suggests a slow electron transfer process.^{36,37}

Indeed, **1** could be readily oxidized by 1 equiv FcPF_6 to afford the Ni^{III} complex $[(^t\text{BuMe}_2\text{tacn})\text{Ni}^{\text{III}}(\text{cycloneophyl})]\text{-PF}_6$ (**2**) in 92% yield (Figure 2b). Notably, the single-crystal X-ray structure of **2** shows a five-coordinate Ni^{III} center with an axial bond length, which is 0.11 Å longer than that in $[(\text{Me}_3\text{tacn})\text{Ni}^{\text{III}}(\text{cycloneophyl})]\text{PF}_6$ (2.19 vs 2.08 Å),¹³ indicating a weaker axial binding interaction due to the steric bulk of the *tert*-butyl group (Figure 3b). In addition, the electron paramagnetic resonance (EPR) spectrum of **2** reveals a weaker superhyperfine coupling constant (15.0 G) in the g_z direction compared to that observed for $[(\text{Me}_3\text{tacn})\text{-Ni}^{\text{III}}(\text{cycloneophyl})]\text{PF}_6$ (17.5 G), further supporting a weaker $\text{Ni-N}_{\text{axial}}$ interaction (Figure 4b). Further oxidation of **2** by acetylferrocenium hexafluorophosphate (AcFcPF_6) resulted in a diamagnetic Ni^{IV} complex (**3**) that persists in solution for 24 h at -60 °C (Figures S46–S50). At elevated temperatures, **3** undergoes rapid reductive elimination to afford the solvento Ni^{II} complex $[(^t\text{BuMe}_2\text{tacn})\text{Ni}^{\text{II}}(\text{MeCN})_3](\text{PF}_6)_2$ (**4**) and a quantitative amount of 1,1-dimethylbenzocyclobutene (**5**, Figure 5). Attempts to crystallize **3** at -60 °C led to the

cycloneophyl Ni complexes supported by the $^t\text{BuMe}_2\text{tacn}$ ligand is significantly reduced vs those supported by Me_3tacn . While $[(\text{Me}_3\text{tacn})\text{Ni}^{\text{III}}(\text{cycloneophyl})]\text{PF}_6$ is stable in solution for days, **2** fully decomposes in MeCN within a day to yield **5**. Similarly, $[(\text{Me}_3\text{tacn})\text{Ni}^{\text{IV}}(\text{cycloneophyl})\text{MeCN}](\text{PF}_6)_2$ is isolable at low temperatures, while **3** is not stable in the solid state. The stability difference is attributed to the weakened electron-donating ability of the amine arm bearing the bulky *tert*-butyl group, and therefore we posit the corresponding high-valent Ni complexes are more prone to reductive elimination.

Oxidative Reactivity of 1. Encouraged by the enhanced reactivity of the high-valent Ni cycloneophyl complexes supported by $^t\text{BuMe}_2\text{tacn}$, we investigated the aerobically induced reactivity of **1** to generate new C–C or C–O bond formation products. Indeed, exposure of **1** to dry O_2 results in rapid formation of benzocyclobutene (**5**) in up to 95% yield in MeCN, or a combined yield of oxygenated products (**6–9**) in up to 21% in 2-MeTHF after acidic workup (Table 1). Notably, the polarity of the solvent plays an important role in determining the chemoselectivity.^{38–40} In polar solvents such as MeCN and DMF, **5** forms predominantly. On the other hand, in weakly polar or nonpolar solvents such as 2-MeTHF and toluene, appreciable amounts of oxygenated products **6–9** are formed. To further enhance the selectivity toward the oxygenated products, we tested the effect of temperature on chemoselectivity in toluene or 2-MeTHF (Table S5), and the formation of C–O products **6–9** was favored at lower temperatures. However, we reasoned that the wide distribution of oxygenated products is a result of overoxidation in the presence of excess amount of oxygen, which complicated the interpretation of the reactivity results. In addition, use of stoichiometric amounts of O_2 did not significantly improve the yields and selectivity for C–O products (Table S6).

Therefore, we hypothesized that the use of another oxidant would alleviate overoxidation side reactions and lead to the selective formation of a single oxygenated species. We proceeded to use hydrogen peroxide as a dioxygen surrogate for ease of accurate measurement, as well as its wide availability and low cost. Interestingly, when only 0.5 equiv of H_2O_2 was added to a solution of **1** in 2-MeTHF at -78 °C, we retrieved 50% *tert*-butylbenzene (**10**) derived from the direct protodemetalation of remaining **1** in the solution, indicating a stoichiometry of 1:1 **1**: H_2O_2 during the reaction (Table 2).

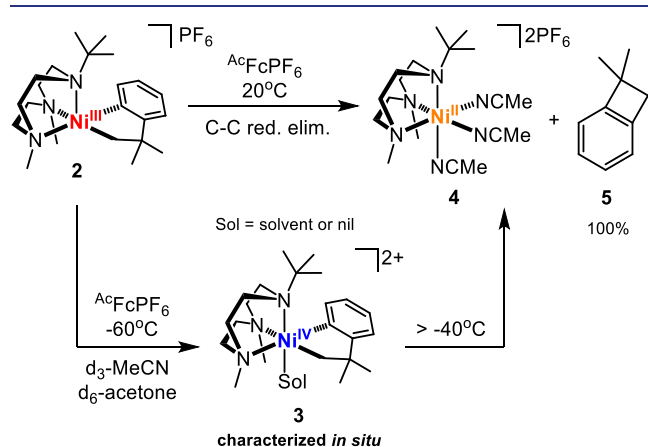


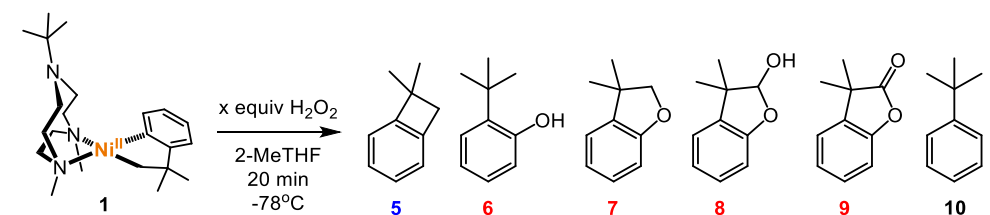
Figure 5. Reaction of **2** with 1 equiv AcFcPF_6 .

decomposition of the Ni^{IV} complex, likely due to its instability in the solid state. By comparison, the stability of high-valent

Table 1. Aerobic Reactivity of Complex **1** in Various Solvents^{a,b}

solvent	dielectric constant	5 (%)	6 (%)	7 (%)	8 (%)	9 (%)	sum (%)	total C–Os (%) ^c	C–Os/C–C ^d
MeCN	36.64	95 ± 3	<1	<1	<1	<1	95	<1	<0.01
DMF	38.25	84 ± 2	<1	1 ± 1	<1	<1	85	1	0.01
THF	7.52	39 ± 2	<1	2 ± 1	5 ± 1	4 ± 1	50	11	0.28
2-MeTHF	6.97	38 ± 1	1 ± 1	5 ± 1	9 ± 1	6 ± 1	59	21	0.55
toluene	2.38	36 ± 1	6 ± 1	3 ± 1	4 ± 1	3 ± 1	52	16	0.44

^aReaction conditions: **1** (0.0049 mmol, 1.0 equiv), trimethoxybenzene (1.0 equiv), 1.5 mL solvent, dry O_2 (1 atm), 5 min, 21 °C. ^bYields were determined by GC-FID upon acidic workup, using 1,3,5-trimethoxybenzene as the internal standard and a calibration curve. ^cTotal C–Os yield = sum of yields of **6**, **7**, **8**, and **9**. ^dC–Os/C–C ratio = (**6** + **7** + **8** + **9**)/**5**.

Table 2. Dependence of Product Distribution on the Amount of H₂O₂ Used^{a,b}


H ₂ O ₂ equiv	5 (%)	6 (%)	7 (%)	8 (%)	9 (%)	10 (%)	sum (%)	total C–O pdts (%) ^c
0.5	2 ± 1	33 ± 1	<1	<1	<1	50 ± 1	85	33
1	6 ± 1	61 ± 1	<1	<1	<1	13 ± 3	80	61
2	4 ± 1	9 ± 3	18 ± 2	5 ± 2	<1	<1	36	32
3	4 ± 1	5 ± 2	18 ± 2	6 ± 1	<1	<1	33	29
4	3 ± 1	3 ± 1	13 ± 3	6 ± 1	<1	<1	25	22
5	5 ± 1	3 ± 1	16 ± 2	7 ± 1	<1	<1	31	26

^aReaction conditions: **1** (0.0049 mmol, 1.0 equiv), trimethoxybenzene (1.0 equiv), 1.5 mL of 2-MeTHF, H₂O₂, 20 min, –78 °C. ^bYields were determined by GC-FID upon acidic workup, using 1,3,5-trimethoxybenzene as the internal standard and a calibration curve. ^cTotal C–O pdts = sum of yields of **6**, **7**, **8**, and **9**.

Importantly, 2-*tert*-butylphenol (**6**) was observed as the only oxygenated product, which reaches a maximum yield of 61% when 1 equiv of H₂O₂ is used. With an excess amount of H₂O₂ (2–5 equiv), the yield of **6** is reduced dramatically, with the concomitant formation of 3,3-dimethyl-2,3-dihydrobenzofuran (**7**) and 3,3-dimethyl-2,3-dihydrobenzofuran-2-ol (**8**), suggesting that the presence of excess oxidants generates overoxidized products. A similar phenomenon has been reported by Puddephatt and co-workers in a Pd system, where selective oxygen atom insertion into the Pd–aryl bond was observed during the reaction of [Pd(cycloneophyl)(MesN = CHCH = NMe₂)] with H₂O₂.⁴¹

To investigate if similar mechanisms are operating in our system, we scaled up the reaction of complex **1** with 1.05 equiv H₂O₂ in 2-MeTHF at –78 °C in an attempt to isolate any oxygenated Ni complexes. NMR analysis of the dried crude product revealed full consumption of complex **1** and the formation of a new species. Gratifyingly, recrystallization of the product in a THF/pentane solution afforded the complex (^tBuMe₂tacn)Ni^{II}(–CH₂CMe₂-*o*-C₆H₄O–) (**11**) as orange crystals in 38% yield (Figure 6). To the best of our knowledge, this is the first observation that hydrogen peroxide can act as an oxygen atom transfer reagent to afford an isolable oxygenated Ni complex, in an oxygenase-like process. Notably, N₂O is usually required as the oxygen atom transfer reagent for Ni complexes, with much longer reaction times being necessary.^{42–46} In our case, the formation of the cycloether product **7** could be generated upon the oxidatively induced reductive elimination from the nickelacycloether **11**. Alternatively, oxidation of **11** followed by a second C–O reductive elimination in the presence of hydroxide could lead to the formation of 2-(1-hydroxy-2-methylpropan-2-yl)phenol (**12**), which was indeed observed under aerobic oxidation conditions (Table S6). Since it has been reported that Ni complexes catalyze the oxidation of alcohols to ketones or aldehydes,^{47,48} **12** can be converted into the corresponding aldehyde by the presence of (^tBuMe₂tacn)Ni complexes and excess oxidants. Spontaneous ring-chain tautomerism of the aldehyde then affords **8** in its cyclized form, and further oxidation of **8** could generate the lactone product **9**.

Mechanistic Studies of the Oxidation of 1. To probe whether a heterolytic or homolytic cleavage of the peroxide O–O bond occurs during the oxidation of **1**, cumene

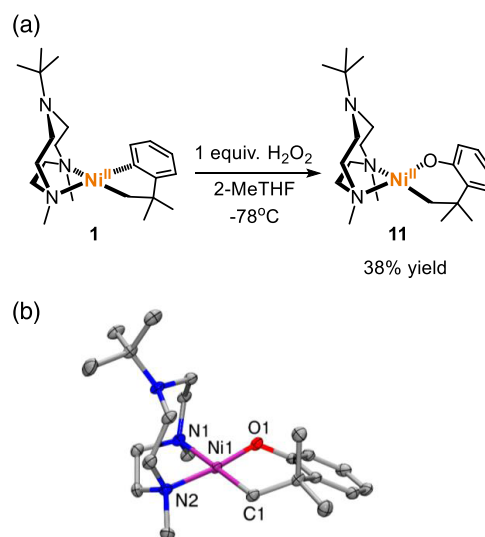


Figure 6. (a) Synthesis of **11**; (b) ORTEP representation (50% probability thermal ellipsoids) of **11**. Selected bond lengths (Å) and angles (°): Ni(1)–O(1) 1.846(2), Ni(1)–N(1) 2.075(2), Ni(1)–C(1) 1.923(2), Ni(1)–N(2) 1.972(2), C(1)–Ni(1)–N(1) 179.5(1), O(1)–Ni(1)–N(2) 172.10(8).

hydroperoxide (CumOOH) was used as the oxidant.^{24,49} Two-electron reduction of CumOOH leads to O–O bond heterolysis, eventually affording α -cumyl alcohol (**13**) after protonation. On the other hand, one-electron reduction of CumOOH promotes O–O bond homolysis and yields acetophenone (**14**) through loss of a methyl radical. When **1** was reacted with 1 equiv CumOOH in 2-MeTHF at –78 °C, **5** and **6** were formed in 2 ± 1% and 50 ± 1% yields upon acidic workup, respectively, similar to the reaction of **1** with H₂O₂ (Table S15). In the same reaction mixture, **13** could be observed by GCMS in 95% yield, while **14** was not detected. The exclusive observation of **13** suggests a clean O–O bond heterolysis and therefore a two-electron oxidation of **1** by CumOOH. When *meta*-chloroperbenzoic acid (*m*CPBA) was used instead of CumOOH, exclusive formation of *meta*-chlorobenzoic acid, but not chlorobenzene, was observed, also suggesting O–O bond heterolysis (Table S13).⁵⁰ As a result, we propose that a Ni^{IV}-hydroxo intermediate (**16**) was formed

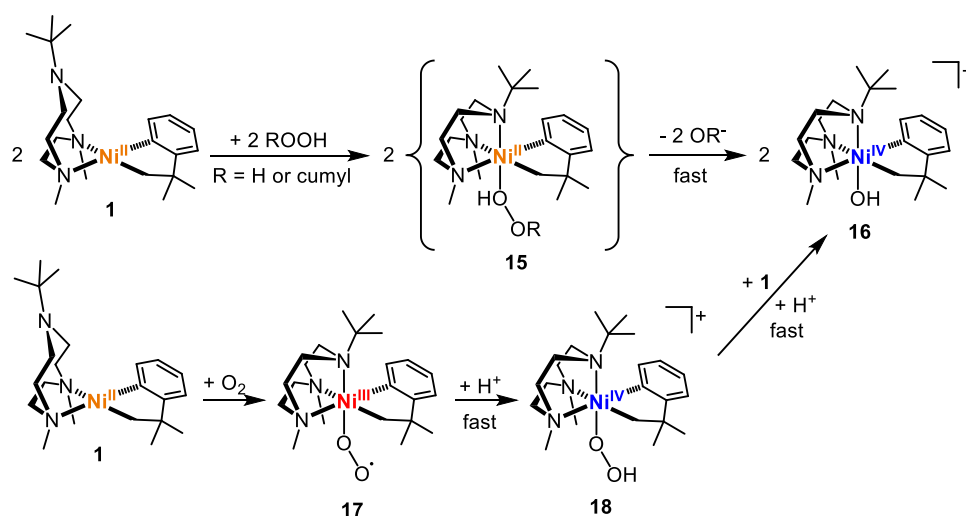


Figure 7. Proposed mechanisms of oxidation of **1** by hydroperoxides or O₂.

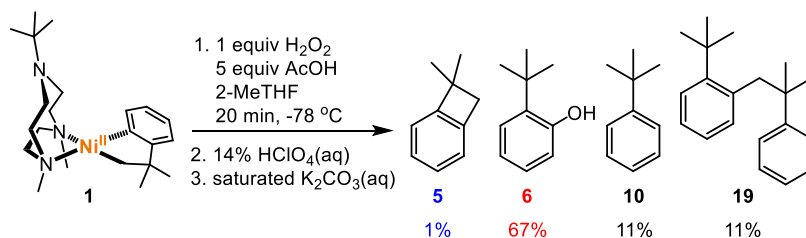


Figure 8. Reaction of **1** with H₂O₂ in the presence of 5 equiv AcOH.

upon the reaction of **1** and hydroperoxides (Figure 7). Notably, the reaction of CumOOH with **1** in MeCN at ambient temperature also showed exclusive formation of **13**, suggesting the general intermediacy of **16**, regardless of the choice of solvent and temperature (Tables S16 and S17).

When 0.25 equiv of O₂ was reacted with **1**, 33% of **10** was retrieved after acidic workup, whereas only a trace amount of **10** could be observed when 0.5 equiv of O₂ was used (Table S6). Since the amount of **10** observed upon acidic workup represents the amount of unreacted **1** remaining in solution, the obtained yield of **10** suggests an ~2:1 **1**:O₂ stoichiometry for the oxidation of **1** and indicative of a two-electron process. This is consistent with previously reported aerobic mechanisms in a relevant Pd system,²⁴ and therefore we tentatively propose a similar pathway that involves the formation of species **16** (Figure 7). The full consumption of **1** with 0.5 equiv O₂ underlines the fast reaction of **1** with O₂,⁵¹ in contrast to reports of catalytic C–H activation reactions in which O₂ was used in great excess or at elevated pressures.^{6,52}

Mechanistic Studies of the Reductive Elimination from Ni^{IV} Intermediate. Since the observed chemoselectivity is heavily dependent on the choice of solvent, we then probed whether the dissociation of the hydroxo group could play a role in determining the selectivity. We hypothesize that if there is a preequilibrium between **16** and **3** through hydroxide coordination and dissociation, the presence of a Lewis or Brønsted acid should scavenge the free hydroxide in solution, rendering more selective formation of **5** due to the lack of a C–O coupling partner. To examine the hypothesis, we tested the effect of additives in C–O bond-forming reactions in 2-MeTHF at –78 °C. Despite the strong Lewis acidity of scandium trifluoromethanesulfonate (Sc(OTf)₃), the reaction

of **1** and H₂O₂ in the presence of 5 equiv Sc(OTf)₃ showed similar yields of **5** and **6** (Table S14). The use of the stronger Brønsted acid trifluoroacetic acid (TFA) led to exclusive protodemetalation of complex **1**. On the other hand, upon addition of a weaker Brønsted acid AcOH (1–5 equiv), the formation of **5** was significantly inhibited, with an increase in the yield of **6** up to 67%, affording the highest yield of **6** among all conditions (Figure 8). Interestingly, another species bearing two connected *tert*-butylbenzene units (**19**) was also observed in 11% yield, suggesting a small extent of organometallic ligand exchange in a weakly acidic environment. Moreover, addition of trimethylamine or boronic acid did not have a significant impact on the yield of **6**. Finally, increasing the concentration of free hydroxide in solution via addition of 5 equiv NMe₄OH lowered the yield of **6** by 15%, while addition of 1 equiv pyridine, a competitive nonsolvent ligand, did not significantly change the yield and distribution of products (Table S14). Overall, these results argue against hydroxide dissociation from **16** under C–O bond-forming conditions in 2-MeTHF at low temperatures. This hypothesis was further probed by isotope labeling experiments using hydrogen peroxide in the presence of excess water. Interestingly, no significant ¹⁸O incorporation into **6** (0.2 ± 0.1%, where the natural abundance level of ¹⁸O is 0.2%) could be observed upon the reaction of **1** and H₂¹⁶O₂ along with 70 equiv H₂¹⁸O (Table S19). On the other hand, ¹⁸O enrichment of **6** up to 95.2 ± 0.3% was observed when H₂¹⁸O₂ (>90% purity) was used along with 70 equiv H₂¹⁶O (Figure 9). In both cases, the extent of ¹⁸O incorporation in **6** is in line with the amount of ¹⁸O in H₂O₂, indicating that the oxygen atom in **6** originates solely from H₂O₂ and that **16** does not undergo oxygen exchange with the surrounding water molecules during the C–O bond-forming reaction. Importantly, the lack

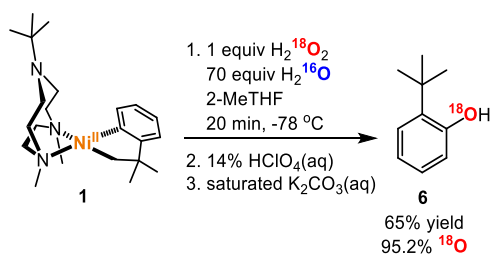


Figure 9. Reaction of **1** with ^{18}O -labeled H_2O_2 in the presence of H_2^{16}O .

of O atom incorporation from water further supports our hypothesis that a Ni^{IV} -oxo/ Ni^{III} -oxyl species does not form in this system (see below) since such high-valent metal-oxo species are known to exchange the O atom with water.^{53–55}

While the Ni^{IV} species **3** was stable at $-78\text{ }^\circ\text{C}$ in solution, the addition of NMe_4OH led to immediate decomposition of **3** and formation of **5** in up to 24% yield and **6** up to 26% yield, highly suggesting the intermediacy of **16**, which is more reactive than **3** (Table S3). Overall, experimental results highly support an inner-sphere $\text{Csp}^2\text{-O}$ reductive elimination between the aryl carbon and the hydroxo group from **16**, leading to the formation of **20**. The phenol group of **20** is rapidly deprotonated and binds to the Ni center, affording **11** as the final product (Figure 10).

Notably, as the reaction temperature is increased, the ratio of C–O product **6** to C–C product **5** decreases 10-fold in both 2-MeTHF and PrCN (Tables S9 and S12), suggesting opposite entropic factors for the two C–O/C–C bond formation processes. Since **3** reductively eliminates to form **5** above $-50\text{ }^\circ\text{C}$, we reasoned that at elevated temperatures, hydroxide dissociation from **16** could take place due to a smaller entropic penalty to generate **3** and subsequently **5** (Figure 10), thus resulting in a lower **6**:**5** ratio. This is

consistent with the decrease of selectivity for the C–O product **6** at temperatures above $-44\text{ }^\circ\text{C}$ in 2-MeTHF. In addition, since dissociation of an anionic ligand is facilitated in more polar solvents,^{39,40,56} we reasoned that the increased polarity of the solvent promotes the dissociation of the hydroxide group, leading to highly selective formation of the C–C product **5** when oxidation occurs in MeCN (Tables 1 and S8).

Kinetic Studies of the Reaction of 1 with H_2O_2 . Kinetic studies were then carried out to gain more mechanistic insight into the oxidation of **1** by H_2O_2 . The rates of formation of the C–O product **11** in 2-MeTHF at $-98\text{ }^\circ\text{C}$ at various concentrations of **1** and H_2O_2 were first investigated using the initial rate method, which revealed that the reaction is first order with respect to both **1** and H_2O_2 in the concentration range from 6.16×10^{-4} to 2.47×10^{-3} M, exhibiting an overall second-order character (Table 3). In addition, the activation

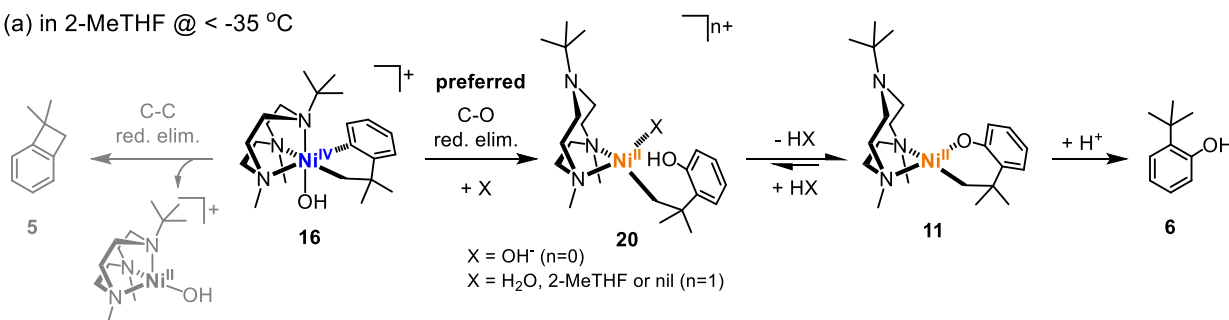
Table 3. Initial Rates of Consumption of **1** (r_1) and Formation of **11** ($r_{\text{C-O}}$) as a Function of Initial Concentration^{a,b}

unit	$[\mathbf{1}]_0$	$[\text{H}_2\text{O}_2]_0$	r_1	$r_{\text{C-O}}$
entry	10^{-4} M	10^{-4} M	10^{-7} M s $^{-1}$	10^{-7} M s $^{-1}$
1	6.16	6.16	16 ± 5	8 ± 1
2	6.16	24.7	51 ± 8	29 ± 9
3	24.7	6.16	48 ± 3	32 ± 13
4	24.7	24.7	192 ± 8	99 ± 6

^aReaction conditions: **1**, 1,3,5-trimethoxybenzene (1.0 equiv to **1**), 2-MeTHF, H_2O_2 , 1 min, $-98\text{ }^\circ\text{C}$. ^bThe consumption of **1** and the formation of **11** were measured as the amount of **10** and **6**, respectively, upon acidic workup.

parameters derived from the Eyring plot over a temperature range from -74 to $-98\text{ }^\circ\text{C}$ reveal a large, negative ΔS^\ddagger value of -47 ± 1 cal $\text{K}^{-1} \text{mol}^{-1}$ and a low ΔH^\ddagger value of 1.7 ± 0.2 kcal

(a) in 2-MeTHF @ $< -35\text{ }^\circ\text{C}$



(b) in MeCN @ RT

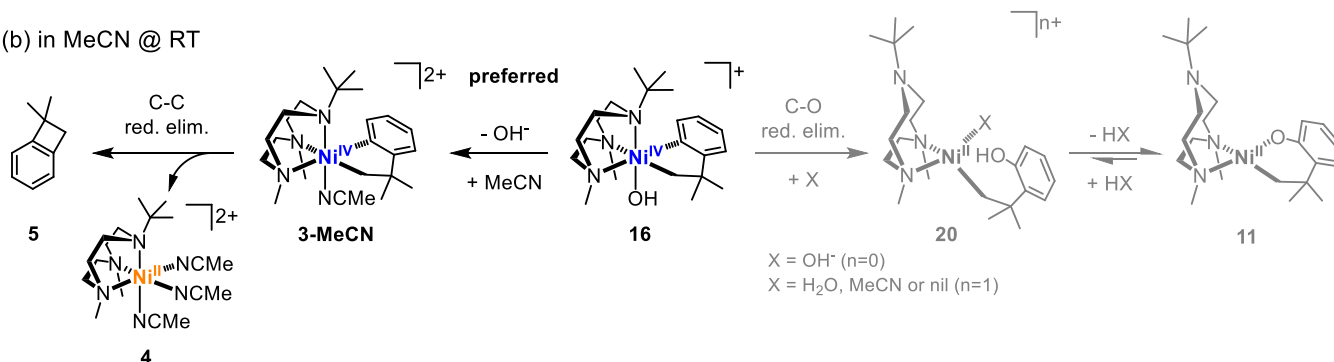


Figure 10. Proposed mechanisms of reductive elimination from the Ni^{IV} intermediate **16** in (a) 2-MeTHF and (b) MeCN. The less preferred reactivity pathways under each condition are shown in gray.

mol^{-1} , corresponding to an overall value of ΔG^\ddagger of 10.5 ± 0.2 kcal mol^{-1} at -85 °C (Table 5) and consistent with an exceptionally fast reaction. Impressively, when extrapolated to room temperature, these kinetic parameters correspond to a pseudo-first-order rate constant in the presence of excess oxidant of ~ 20 s^{-1} , which is similar to the rates observed for cytochrome P450 enzymes and heme peroxidases.^{57–59}

Previous reports have shown that reactions involving H_2O_2 as a direct oxidant usually feature large negative values of ΔS^\ddagger ranging from -125 to -167 J K^{-1} mol^{-1} (-30 to -40 cal K^{-1} mol^{-1}) as a result of a rate-determining bimolecular/associative electron transfer step.^{60,61} Based on the second-order dependence of the oxidation of **1** by H_2O_2 and the large negative value of ΔS^\ddagger , we propose that the formation of the $\text{Ni}^{\text{II}}-\text{H}_2\text{O}_2$ complex **15** is the rate-determining step in the Csp^2-O bond-forming reaction (Figure 7). In fact, the value of ΔS^\ddagger in our system is even more negative than the other reported values, and we reason that this is likely due to the concomitant coordination of the axial *tert*-butyl amine arm to the Ni center, which facilitates the cleavage of the O–O bond and oxidation of the Ni center, further decreasing the number of degrees of freedom and leading to a more negative ΔS^\ddagger .

Similarly, when the reaction of **1** with H_2O_2 was carried out in 79:1 MeCN/2-MeTHF at -41 °C, the rate of formation of the C–C product **5** shows a first-order dependence on both **1** and H_2O_2 (Table 4). However, a positive ΔS^\ddagger value of 29 ± 10

Table 4. Initial Rates of Formation of **5 ($r_{\text{C-C}}$) as a Function of Initial Concentration^a**

unit	$[\mathbf{1}]_0$	$[\text{H}_2\text{O}_2]_0$	$r_{\text{C-C}}$
entry	10^{-5} M	10^{-5} M	10^{-8} M s^{-1}
1	7.73	7.73	31 ± 10
2	7.73	30.9	116 ± 67
3	30.9	7.73	98 ± 24
4	30.9	30.9	430 ± 16

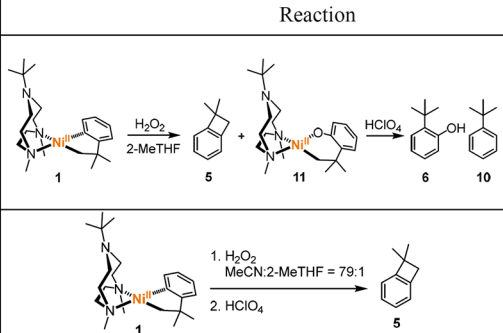
^aReaction conditions: **1**, 1,3,5-trimethoxybenzene (1.0 equiv to **1**), MeCN/2-MeTHF = 79:1, H_2O_2 , 30 s, -41 °C.

cal K^{-1} mol^{-1} and a higher ΔH^\ddagger value of 18 ± 3 kcal mol^{-1} were derived from the Eyring analysis, suggesting a different rate-determining step (Table 5). This could be due to the binding of MeCN molecule(s) to the Ni center in **1**, which is consistent with the more complex CV and NMR data in

MeCN (or MeCN-*d*₃) in comparison to those in THF or C_6D_6 (Figures S6–S19 and S38–S41). DFT calculations also suggest that **31a** and **1b**, both MeCN adducts of **1**, could be accessible energetically at room temperature and thus control the oxidative reactivity (Figure S59). However, we cannot exclude the possibility that the observed positive ΔS^\ddagger value is due to a rate-determining C–C bond formation from a Ni^{IV} intermediate, which can also be modulated by MeCN binding to further promote the reductive elimination step.

The proposed mechanism for the selective Csp^2-O formation was further examined computationally by calculating the reaction energy profile and the relevant transition states for the oxidation and reductive elimination steps (Figure 11). The DFT calculations were carried out employing a B3LYP-D3/LACVP/6-31G** level of theory for the geometry optimization, vibration, and solvation energy calculations. The electronic energies of all optimized structures were reevaluated with B3LYP-D3/LACV3P/cc-pVTZ(-f),^{62–72} as described in the Supporting Information. The initial oxidation of **1** by H_2O_2 via **1-TS** is found to require 11.9 kcal mol^{-1} to furnish the $\text{Ni}^{\text{IV}}-\text{OH}$ intermediate **16**, which is lower in energy than **1** by 2.6 kcal mol^{-1} . Importantly, we have also considered the potential formation of a $\text{Ni}^{\text{IV}}-\text{oxo}/\text{Ni}^{\text{III}}-\text{oxyl}$ species during the oxidation of **1** by H_2O_2 , via the formation of a $\text{Ni}^{\text{II}}-\text{OOH}$ transient species (**315a-dH**, Figure S59) followed by heterolytic O–O bond cleavage, yet such a $\text{Ni}^{\text{II}}-\text{OOH}$ species was calculated to be very high in energy (50.9 kcal mol^{-1} vs **1**) and thus the formation of a $\text{Ni}^{\text{IV}}-\text{oxo}/\text{Ni}^{\text{III}}-\text{oxyl}$ species is considered to be disfavored in this system. This hypothesis is in line with the isotopic labeling experiments that suggest a $\text{Ni}^{\text{IV}}-\text{oxo}/\text{Ni}^{\text{III}}-\text{oxyl}$ species is not involved in the C–O bond formation step since no O incorporation from water into the C–O product **6** is observed (Figure 9). The intermediate **16** can then undergo Csp^2-O reductive elimination, and the calculated transition state **16-TS_O** corresponds to a barrier of 16.6 kcal mol^{-1} , which is 1.5 kcal mol^{-1} lower than the competing $\text{Csp}^2-\text{Csp}^3$ reductive elimination via the transition state **16-TS_C** (Figure 11). After the Csp^2-O reductive elimination, which is favored thermodynamically, subsequent rearrangement and deprotonation by hydroxide will give **11**, which generates **6** upon acidic workup. It is worth mentioning that while the calculated transition state **1-TS** for the oxidation step leading to the formation of **16** is calculated to be slightly lower than the transition state **16-TS_O** for the Csp^2-O

Table 5. Kinetic Parameters for the Oxidation of **1 by H_2O_2**

Reaction	ΔH^\ddagger (kcal/mol)	ΔS^\ddagger (cal/mol K)	ΔG^\ddagger (kcal/mol)	
	Consumption of 1 ^a	1.0 ± 0.2	-50 ± 1	10.3 ± 0.2 @ -85 °C
	Formation of 11 ^a	1.7 ± 0.2	-47 ± 1	10.5 ± 0.2 @ -85 °C
	Formation of 5 ^a	2.7 ± 0.5	-49 ± 3	11.7 ± 0.7 @ -85 °C
Formation of 5 ^b	18 ± 3	29 ± 10	11 ± 3 @ -35 °C	

^aThe consumption of **1** and the formation of **11** were measured as the amount of **10** and **6**, respectively, upon acidic workup. Reaction conditions: $[\mathbf{1}]_0 = [\text{H}_2\text{O}_2]_0 = 2.47 \times 10^{-3}$ M, temperature ranging from -74 to -98 °C in 2-MeTHF. ^bReaction conditions: $[\mathbf{1}]_0 = [\text{H}_2\text{O}_2]_0 = 7.73 \times 10^{-5}$ M, temperature ranging from -29 to -41 °C in a solution of MeCN/2-MeTHF = 79:1.

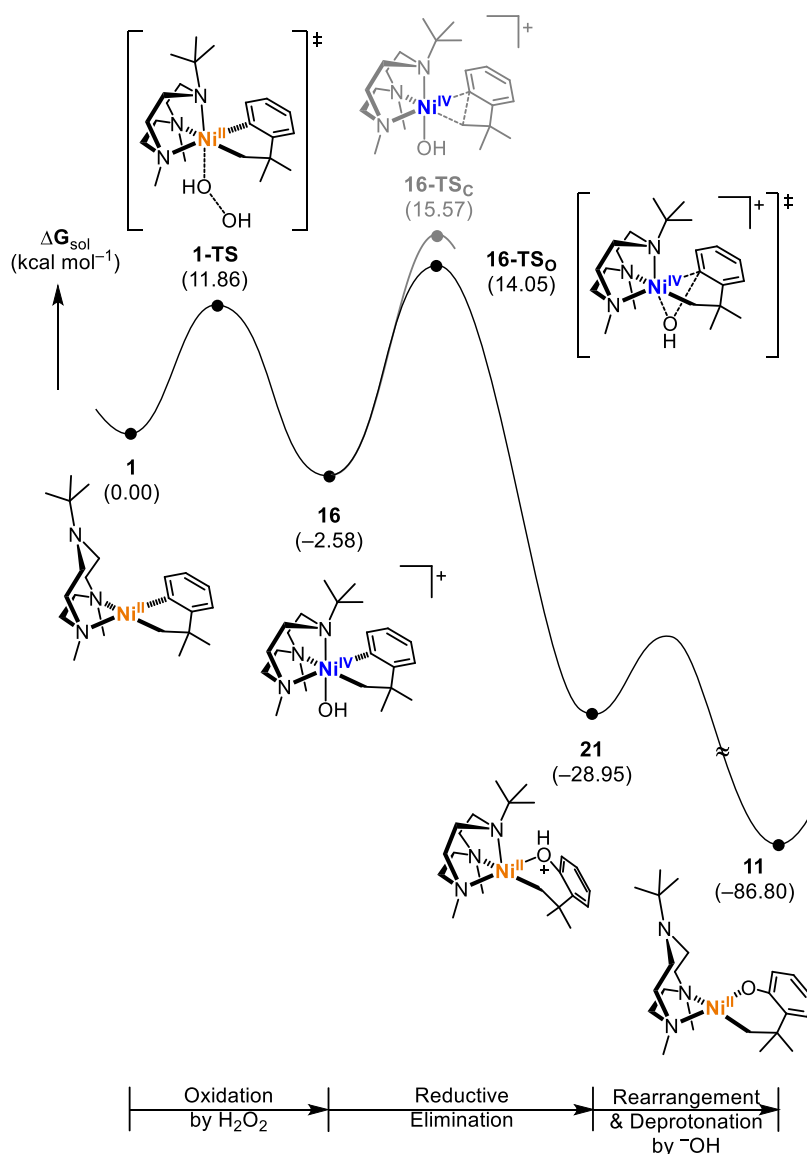


Figure 11. Energy profile of the proposed mechanism for the oxidation of **1** by H_2O_2 in 2-MeTHF.

reductive elimination, the oxidation step via **1-TS** could still be the rate-limiting step (as suggested experimentally) since this oxidation step is a bimolecular process, while the $\text{Csp}^2\text{-O}$ reductive elimination is an intramolecular process that is not limited by the rate of diffusion. Overall, the DFT calculations strongly support the proposed mechanism in which the $\text{Ni}^{\text{IV}}\text{-OH}$ complex **16** is formed via heterolytic cleavage of H_2O_2 , followed by the selective formation of the $\text{Csp}^2\text{-O}$ bond via reductive elimination. Finally, the selective formation of the C–O product may actually be due to the lack of formation of a $\text{Ni}^{\text{IV}}\text{-oxo}/\text{Ni}^{\text{III}}\text{-oxyl}$ species, which is known to rapidly undergo unspecific hydrogen atom transfer (HAT) reactivity.^{53–55} Thus, we would like to put forward the proposal that avoiding the formation of $\text{Ni}^{\text{IV}}\text{-oxo}/\text{Ni}^{\text{III}}\text{-oxyl}$ transient species is key to promote selective C–O reductive elimination for productive transformations.

CONCLUSIONS

Herein, we report the detailed study of oxidatively induced $\text{Csp}^2\text{-O}$ and $\text{Csp}^2\text{-Csp}^3$ bond formation upon the reaction of the organometallic Ni complex ($t\text{BuMe}_2\text{tacn}$)-

$\text{Ni}^{\text{II}}(\text{cycloneophyl})$ (**1**) with peroxides or O_2 . By weakening the interaction of the Ni center with one of the amine donors by installing a bulky *tert*-butyl substituent on the ligand, we were able to accomplish oxidatively induced selective $\text{Csp}^2\text{-O}$ bond formation in good yields using green oxidants such as O_2 and H_2O_2 . Detailed mechanistic studies were conducted to probe the intermediacy of Ni^{IV} intermediates and their reactivity. Isotope labeling experiments suggest the generation of a high-valent Ni-oxygen species via an inner-sphere mechanism, while kinetic studies of the exceptionally fast $\text{Csp}^2\text{-O}$ bond-forming reaction reveal a first-order dependence on both Ni^{II} complex and H_2O_2 , and thus an overall second-order reaction. Eyring analysis further suggests that the oxidation of the Ni^{II} complex by H_2O_2 is the rate-determining step, which can be modulated by the presence of coordinating solvents. Moreover, DFT calculations were employed to provide insights into the molecular structure of transition states and the source of the observed C–O vs C–C chemoselectivity. This study thus shows that the control of the axial amine arm is essential for both the oxidation of organometallic Ni^{II} species with mild oxidants, as well as the

subsequent C–O bond-forming reductive elimination from a high-valent Ni^{IV}–OH intermediate, leading to a system that functionally mimics oxygenase and peroxidase metalloenzymes. Finally, we would like to put forward the proposal that avoiding the formation of Ni^{IV}–oxo/Ni^{III}–oxyl transient species is key to promote selective C–O reductive elimination for productive transformations promoted by high-valent Ni systems.

■ ASSOCIATED CONTENT

SI Supporting Information

The Supporting Information is available free of charge at <https://pubs.acs.org/doi/10.1021/jacs.3c01012>.

Synthetic details; spectroscopic and electrochemical characterization; mechanistic and kinetic studies; computational details; and crystallographic data (PDF)

Accession Codes

CCDC 2181749, 2181757–2181758, and 2181903 contain the supplementary crystallographic data for this paper. These data can be obtained free of charge via www.ccdc.cam.ac.uk/data_request/cif, or by emailing data_request@ccdc.cam.ac.uk, or by contacting The Cambridge Crystallographic Data Centre, 12 Union Road, Cambridge CB2 1EZ, UK; fax: +44 1223 336033.

■ AUTHOR INFORMATION

Corresponding Authors

Mu-Hyun Baik – Department of Chemistry, Korea Advanced Institute of Science and Technology (KAIST), Daejeon 34141, Republic of Korea; Center for Catalytic Hydrocarbon Functionalizations, Institute for Basic Science (IBS), Daejeon 34141, Republic of Korea; orcid.org/0000-0002-8832-8187; Email: mbaik2805@kaist.ac.kr

Liviu M. Mirica – Department of Chemistry, University of Illinois at Urbana-Champaign, Urbana, Illinois 61801, United States; orcid.org/0000-0003-0584-9508; Email: mirica@illinois.edu

Authors

Chi-Herng Hu – Department of Chemistry, University of Illinois at Urbana-Champaign, Urbana, Illinois 61801, United States

Seoung-Tae Kim – Department of Chemistry, Korea Advanced Institute of Science and Technology (KAIST), Daejeon 34141, Republic of Korea; Center for Catalytic Hydrocarbon Functionalizations, Institute for Basic Science (IBS), Daejeon 34141, Republic of Korea

Complete contact information is available at: <https://pubs.acs.org/10.1021/jacs.3c01012>

Notes

The authors declare no competing financial interest.

■ ACKNOWLEDGMENTS

The authors thank the Taiwan UIUC fellowship (1070055211A to C.-H.H.), the National Science Foundation (CHE-1925751 and CHE-2155160 to L.M.M.), and the Institute for Basic Science in Korea (IBS-R010-A1 to M.-H.B.) for financial support of this research. They also thank Dr. Toby Woods for help with X-ray crystal structure analysis, and Dr. Lingyang Zhu for help with low-temperature NMR experiments.

■ REFERENCES

- (1) Ertl, P.; Schuhmann, T. A Systematic Cheminformatics Analysis of Functional Groups Occurring in Natural Products. *J. Nat. Prod.* **2019**, *82*, 1258–1263.
- (2) Lehn, J. M. Supramolecular polymer chemistry- scope and perspectives. *Polym. Int.* **2002**, *51*, 825–839.
- (3) Kristufek, S. L.; Wacker, K. T.; Tsao, Y. Y. T.; Su, L.; Wooley, K. L. Monomer design strategies to create natural product-based polymer materials. *Nat. Prod. Rep.* **2017**, *34*, 433–459.
- (4) Enthaler, S.; Company, A. Palladium-catalysed hydroxylation and alkoxylation. *Chem. Soc. Rev.* **2011**, *40*, 4912–4924.
- (5) Lyons, T. W.; Sanford, M. S. Palladium-Catalyzed Ligand-Directed C–H Functionalization Reactions. *Chem. Rev.* **2010**, *110*, 1147–1169.
- (6) Li, Z.; Wang, Z.; Chekshin, N.; Qian, S. Q.; Qiao, J. X.; Cheng, P. T.; Yeung, K. S.; Ewing, W. R.; Yu, J. Q. A tautomeric ligand enables directed C–H hydroxylation with molecular oxygen. *Science* **2021**, *372*, 1452–1457.
- (7) Li, Z.; Park, H. S.; Qiao, J. X.; Yeung, K. S.; Yu, J. Q. Ligand-Enabled C–H Hydroxylation with Aqueous H₂O₂ at Room Temperature. *J. Am. Chem. Soc.* **2022**, *144*, 18109–18116.
- (8) Gandeepan, P.; Müller, T.; Zell, D.; Cera, G.; Warratz, S.; Ackermann, L. 3d Transition Metals for C–H Activation. *Chem. Rev.* **2019**, *119*, 2192–2452.
- (9) Khake, S. M.; Chatani, N. Chelation-Assisted Nickel-Catalyzed C–H Functionalizations. *Trends Chem.* **2019**, *1*, 524–539.
- (10) Khake, S. M.; Chatani, N. Nickel-Catalyzed C–H Functionalization Using A Non-directed Strategy. *Chem* **2020**, *6*, 1056–1081.
- (11) Zheng, B.; Tang, F. Z.; Luo, J.; Schultz, J. W.; Rath, N. P.; Mirica, L. M. Organometallic Nickel(III) Complexes Relevant to Cross-Coupling and Carbon-Heteroatom Bond Formation Reactions. *J. Am. Chem. Soc.* **2014**, *136*, 6499–6504.
- (12) Zhou, W.; Schultz, J. W.; Rath, N. P.; Mirica, L. M. Aromatic Methoxylation and Hydroxylation by Organometallic High-Valent Nickel Complexes. *J. Am. Chem. Soc.* **2015**, *137*, 7604–7607.
- (13) Watson, M. B.; Rath, N. P.; Mirica, L. M. Oxidative C–C Bond Formation Reactivity of Organometallic Ni(II), Ni(III), and Ni(IV) Complexes. *J. Am. Chem. Soc.* **2017**, *139*, 35–38.
- (14) Smith, S. M.; Planas, O.; Gomez, L.; Rath, N.; Ribas, X.; Mirica, L. M. Aerobic C–C and C–O bond formation reactions mediated by high-valent nickel species. *Chem. Sci.* **2019**, *10*, 10366–10372.
- (15) Higgs, A. T.; Zinn, P. J.; Simmons, S. J.; Sanford, M. S. Oxidatively Induced Carbon-Halogen Bond-Forming Reactions at Nickel. *Organometallics* **2009**, *28*, 6142–6144.
- (16) Camasso, N. M.; Sanford, M. S. Design, synthesis, and carbon-heteroatom coupling reactions of organometallic nickel(IV) complexes. *Science* **2015**, *347*, 1218–1220.
- (17) Meucci, E. A.; Ariafard, A.; Canty, A. J.; Kampf, J. W.; Sanford, M. S. Aryl–Fluoride Bond-Forming Reductive Elimination from Nickel(IV) Centers. *J. Am. Chem. Soc.* **2019**, *141*, 13261–13267.
- (18) Roberts, C. C.; Camasso, N. M.; Bowes, E. G.; Sanford, M. S. Impact of Oxidation State on Reactivity and Selectivity Differences between Nickel(III) and Nickel(IV) Alkyl Complexes. *Angew. Chem., Int. Ed.* **2019**, *58*, 9104–9108.
- (19) Roberts, C. C.; Chong, E.; Kampf, J. W.; Canty, A. J.; Ariafard, A.; Sanford, M. S. Nickel(II/IV) Manifold Enables Room-Temperature C(sp³)-H Functionalization. *J. Am. Chem. Soc.* **2019**, *141*, 19513–19520.
- (20) Cloutier, J. P.; Zargarian, D. Functionalization of the Aryl Moiety in the Pincer Complex (NCN)(NiBr₂)-Br-III: Insights on Ni-III-Promoted Carbon-Heteroatom Coupling. *Organometallics* **2018**, *37*, 1446–1455.
- (21) Na, H.; Mirica, L. M. Deciphering the mechanism of the Ni-photocatalyzed C–O cross-coupling reaction using a tridentate pyridinophane ligand. *Nat. Commun.* **2022**, *13*, No. 1313.
- (22) Zhang, S. K.; Struwe, J.; Hu, L. R.; Ackermann, L. Nickel-electrocatalyzed C–H Alkoxylation with Secondary Alcohols: Oxidation-Induced Reductive Elimination at Nickel(III). *Angew. Chem., Int. Ed.* **2020**, *59*, 3178–3183.

- (23) Furuya, T.; Kamlet, A. S.; Ritter, T. Catalysis for fluorination and trifluoromethylation. *Nature* **2011**, *473*, 470–477.
- (24) Khusnutdinova, J. R.; Rath, N. P.; Mirica, L. M. The Aerobic Oxidation of a Pd(II) Dimethyl Complex Leads to Selective Ethane Elimination from a Pd(III) Intermediate. *J. Am. Chem. Soc.* **2012**, *134*, 2414–2422.
- (25) Qu, F. R.; Khusnutdinova, J. R.; Rath, N. P.; Mirica, L. M. Dioxygen activation by an organometallic Pd(II) precursor: formation of a Pd(IV)-OH complex and its C-O bond formation reactivity. *Chem. Commun.* **2014**, *50*, 3036–3039.
- (26) Smith, S. M.; Rath, N. P.; Mirica, L. M. Axial Donor Effects on Oxidatively Induced Ethane Formation from Nickel-Dimethyl Complexes. *Organometallics* **2019**, *38*, 3602–3609.
- (27) Chaudhuri, P.; Wieghardt, K. The Chemistry of 1,4,7-Triazacyclononane and Related Tridentate Macrocyclic-Compounds. In *Progress in Inorganic Chemistry*; John Wiley & Sons, 1987; Vol. 35, pp 329–436.
- (28) Sibbons, K. F.; Shastri, K.; Watkinson, M. The application of manganese complexes of ligands derived from 1,4,7-triazacyclononane in oxidative catalysis. *Dalton Trans.* **2006**, 645–661.
- (29) Tang, F.; Qu, F.; Khusnutdinova, J. R.; Rath, N. P.; Mirica, L. M. Structural and Reactivity Comparison of Analogous Organometallic Pd(III) and Pd(IV) Complexes. *Dalton Trans.* **2012**, *41*, 14046–14050.
- (30) Grenz, A.; Ceccarelli, S.; Bolm, C. Synthesis and application of novel catalytically active polymers containing 1,4,7-triazacyclononanes. *Chem. Commun.* **2001**, 1726–1727.
- (31) Pickel, T. C.; Karahalil, G. J.; Buru, C. T.; Bacs, J.; Scarborough, C. C. Synthesis of Previously Inaccessible Derivatives of 1,4,7-Tri-R-1,4,7-Triazacyclononane, Including Chiral Examples, and a Rapid Synthesis of the HCl Salts of H3tacn and H4dtne. *Eur. J. Org. Chem.* **2018**, *2018*, 6876–6889.
- (32) Campora, J.; Conejo, M. D.; Mereiter, K.; Palma, P.; Perez, C.; Reyes, M. L.; Ruiz, C. Synthesis of dialkyl, diaryl and metallacyclic complexes of Ni and Pd containing pyridine, alpha-diimines and other nitrogen ligands crystal structures of the complexes cis-NiR(2)py(2) (R = benzyl, mesityl). *J. Organomet. Chem.* **2003**, *683*, 220–239.
- (33) Schultz, J. W.; Fuchigami, K.; Zheng, B.; Rath, N. P.; Mirica, L. M. Isolated Organometallic Nickel(III) and Nickel(IV) Complexes Relevant to Carbon-Carbon Bond Formation Reactions. *J. Am. Chem. Soc.* **2016**, *138*, 12928–12934.
- (34) Khusnutdinova, J. R.; Rath, N. P.; Mirica, L. M. The Conformational Flexibility of the Tetradentate Ligand ¹⁸N4 is Essential for the Stabilization of (¹⁸N4)Pd^{III} Complexes. *Inorg. Chem.* **2014**, *53*, 13112–13129.
- (35) Tang, F.; Park, S.; Rath, N. P.; Mirica, L. M. Electronic versus steric effects of pyridinophane ligands on Pd(III) complexes. *Dalton Trans.* **2018**, *47*, 1151–1158.
- (36) Geiger, W. E. Structural Changes Accompanying Metal Complex Electrode Reactions. In *Progress in Inorganic Chemistry*; John Wiley & Sons, Inc., 1985; pp 275–352.
- (37) Khusnutdinova, J. R.; Luo, J.; Rath, N. P.; Mirica, L. M. Late First-Row Transition Metal Complexes of a Tetradentate Pyridinophane Ligand: Electronic Properties and Reactivity Implications. *Inorg. Chem.* **2013**, *52*, 3920–3932.
- (38) Spingler, B.; Schnidrig, S.; Todorova, T.; Wild, F. Some thoughts about the single crystal growth of small molecules. *CrystEngComm* **2012**, *14*, 751–757.
- (39) Williams, B. S.; Holland, A. W.; Goldberg, K. I. Direct observation of C-O reductive elimination from Pt(IV). *J. Am. Chem. Soc.* **1999**, *121*, 252–253.
- (40) Williams, B. S.; Goldberg, K. I. Studies of reductive elimination reactions to form carbon-oxygen bonds from Pt(IV) complexes. *J. Am. Chem. Soc.* **2001**, *123*, 2576–2587.
- (41) Behnia, A.; Boyle, P. D.; Blacquiere, J. M.; Puddephatt, R. J. Selective Oxygen Atom Insertion into an Aryl-Palladium Bond. *Organometallics* **2016**, *35*, 2645–2654.
- (42) Matsunaga, P. T.; Hillhouse, G. L.; Rheingold, A. L. Oxygen-Atom Transfer from Nitrous-Oxide to a Nickel Metallacycle - Synthesis, Structure, and Reactions of (2,2'-Bipyridine)Ni-(OCH2CH2CH2CH2). *J. Am. Chem. Soc.* **1993**, *115*, 2075–2077.
- (43) Koo, K. M.; Hillhouse, G. L.; Rheingold, A. L. Oxygen-Atom Transfer from Nitrous Oxide to an Organonickel(II) Phosphine Complex. Syntheses and Reactions of New Nickel(II) Aryloxides and the Crystal-Structure of [cyclic] (Me2PCH2CH2PMe2)Ni(O-o-C6H4CMe2CH2). *Organometallics* **1995**, *14*, 456–460.
- (44) Le Vaillant, F.; Reijerse, E. J.; Leutzsch, M.; Cornella, J. Dialkyl Ether Formation at High-Valent Nickel. *J. Am. Chem. Soc.* **2020**, *142*, 19540–19550.
- (45) Le Vaillant, F.; Mateos Calbet, A.; Gonzalez-Pelayo, S.; Reijerse, E. J.; Ni, S.; Busch, J.; Cornella, J. Catalytic synthesis of phenols with nitrous oxide. *Nature* **2022**, *604*, 677–683.
- (46) Ni, S.; Le Vaillant, F.; Mateos-Calbet, A.; Martin, R.; Cornella, J. Ni-Catalyzed Oxygen Transfer from N2O onto sp3-Hybridized Carbons. *J. Am. Chem. Soc.* **2022**, *144*, 18223–18228.
- (47) Weiss, C. J.; Das, P.; Miller, D. L.; Helm, M. L.; Appel, A. M. Catalytic Oxidation of Alcohol via Nickel Phosphine Complexes with Pendant Amines. *ACS Catal.* **2014**, *4*, 2951–2958.
- (48) Ye, D. F.; Liu, Z. Y.; Sessler, J. L.; Lei, C. H. Base-free oxidation of alcohols enabled by nickel(ii)-catalyzed transfer dehydrogenation. *Chem. Commun.* **2020**, *56*, 11811–11814.
- (49) Matsui, T.; Nagano, S.; Ishimori, K.; Watanabe, Y.; Morishima, I. Preparation and Reactions of Myoglobin Mutants Bearing both Proximal Cysteine Ligand and Hydrophobic Distal Cavity: Protein Models for the Active Site of P-450. *Biochemistry* **1996**, *35*, 13118–13124.
- (50) Qiu, Y.; Hartwig, J. F. Mechanism of Ni-Catalyzed Oxidations of Unactivated C(sp3)-H Bonds. *J. Am. Chem. Soc.* **2020**, *142*, 19239–19248.
- (51) Xu, H. W.; Diccianni, J. B.; Katigbak, J.; Hu, C. H.; Zhang, Y. K.; Diao, T. N. Bimetallic C-C Bond-Forming Reductive Elimination from Nickel. *J. Am. Chem. Soc.* **2016**, *138*, 4779–4786.
- (52) Zhang, Y.-H.; Yu, J.-Q. Pd(II)-Catalyzed Hydroxylation of Arenes with 1 atm of O2 or Air. *J. Am. Chem. Soc.* **2009**, *131*, 14654–14655.
- (53) Corona, T.; Pfaff, F. F.; Acuna-Pares, F.; Draksharapu, A.; Whiteoak, C. J.; Martin-Diaconescu, V.; Lloret-Fillol, J.; Browne, W. R.; Ray, K.; Company, A. Reactivity of a Nickel(II) Bis(amidate) Complex with meta-Chloroperbenzoic Acid: Formation of a Potent Oxidizing Species. *Chem. - Eur. J.* **2015**, *21*, 15029–15038.
- (54) Corona, T.; Company, A. Spectroscopically Characterized Synthetic Mononuclear Nickel-Oxygen Species. *Chem. - Eur. J.* **2016**, *22*, 13422–13429.
- (55) Corona, T.; Draksharapu, A.; Padamati, S. K.; Gamba, I.; Martin-Diaconescu, V.; Acuna-Pares, F.; Browne, W. R.; Company, A. Rapid Hydrogen and Oxygen Atom Transfer by a High-Valent Nickel-Oxygen Species. *J. Am. Chem. Soc.* **2016**, *138*, 12987–12996.
- (56) Goldberg, K. I.; Yan, J. Y.; Breitung, E. M. Energetics and Mechanisms of Carbon-Carbon and Carbon-Iodide Reductive Elimination from a Pt(IV) Center. *J. Am. Chem. Soc.* **1995**, *117*, 6889–6896.
- (57) Purdy, M. M.; Koo, L. S.; de Montellano, P. R. O.; Klinman, J. P. Steady-State Kinetic Investigation of Cytochrome P450cam: Interaction with Redox Partners and Reaction with Molecular Oxygen. *Biochemistry* **2004**, *43*, 271–281.
- (58) Rittle, J.; Green, M. T. Cytochrome P450 Compound I: Capture, Characterization, and C-H Bond Activation Kinetics. *Science* **2010**, *330*, 933–937.
- (59) Dunford, H. B. Heme Peroxidase Kinetics. In *Heme Peroxidases*; Raven, E.; Dunford, B., Eds.; The Royal Society of Chemistry, 2015; pp 99–112.
- (60) Barnard, D.; Bateman, L.; Cunneen, J. I. Oxidation of Organic Sulfides. In *Organic Sulfur Compounds*; Pergamon Press, 1961; pp 229–247.
- (61) Nguyen, T. H.; Burnier, J.; Meng, W. The Kinetics of Relaxin Oxidation by Hydrogen-Peroxide. *Pharm. Res.* **1993**, *10*, 1563–1571.

(62) Becke, A. D. Density-functional Exchange-energy Approximation With Correct Asymptotic-behavior. *Phys. Rev. A* **1988**, *38*, 3098–3100.

(63) Lee, C.; Yang, W.; Parr, R. G. Development of the Colle-Salvetti Correlation-Energy Formula Into a Functional of the Electron-Density. *Phys. Rev. B* **1988**, *37*, 785–789.

(64) Grimme, S.; Antony, J.; Ehrlich, S.; Krieg, H. A consistent and accurate ab initio parametrization of density functional dispersion correction (DFT-D) for the 94 elements H-Pu. *J. Chem. Phys.* **2010**, *132*, No. 154104.

(65) Ditchfield, R.; Hehre, W. J.; Pople, J. A. Self-Consistent Molecular-Orbital Methods. IX. An Extended Gaussian-Type Basis for Molecular-Orbital Studies of Organic Molecules. *J. Chem. Phys.* **1971**, *54*, 724–728.

(66) Hehre, W. J.; Lathan, W. A. Self-Consistent Molecular Orbital Methods. XIV. An Extended Gaussian-Type Basis for Molecular Orbital Studies of Organic Molecules. Inclusion of Second Row Elements. *J. Chem. Phys.* **1972**, *56*, 5255–5257.

(67) Rassolov, V. A.; Ratner, M. A.; Pople, J. A.; Redfern, P. C.; Curtiss, L. A. 6-31G* basis set for third-row atoms. *J. Comput. Chem.* **2001**, *22*, 976–984.

(68) Hay, P. J.; Wadt, W. R. Ab initio effective core potentials for molecular calculations. Potentials for the transition metal atoms Sc to Hg. *J. Chem. Phys.* **1985**, *82*, 270–283.

(69) Wadt, W. R.; Hay, P. J. Ab initio Effective Core Potentials for Molecular Calculations. Potentials for Main Group Elements Na to Bi. *J. Chem. Phys.* **1985**, *82*, 284–298.

(70) Hay, P. J.; Wadt, W. R. Ab initio effective core potentials for molecular calculations. Potentials for K to Au including the outermost core orbitals. *J. Chem. Phys.* **1985**, *82*, 299–310.

(71) Dunning, T. H. Gaussian-Basis Sets for Use in Correlated Molecular Calculations. I. The Atoms Boron through Neon and Hydrogen. *J. Chem. Phys.* **1989**, *90*, 1007–1023.

(72) LACV3P**^{*}: a triple-zeta contraction of the LACVP basis set developed by Schrodinger Inc. The main group elements (H-Ar) are calculated employing 6-311G**^{*}.